# Interactions between Organized, Surface-Confined Monolayers and Vapor-Phase Probe Molecules. 7. Comparison of Self-Assembling *n*-Alkanethiol Monolayers Deposited on Gold from Liquid and Vapor Phases

**Orawon Chailapakul,† Li Sun,‡ Chuanjing Xu,† and Richard M. Crooks*,†**

*Contribution from the Department of Chemistry, University of New Mexico, Albuquerque, New Mexico 87131*

*Received August 10, 1993®*

**Abstract:** We report a comparative study of the structure and chemistry of methyl-terminated *n*-alkanethiol self-assembling monolayers (SAMs) formed from liquid and vapor phases. Three different SAMs are considered: Au/$HS(CH_2)_nCH_3$, $n$ = 5, 11, and 15. Liquid-phase-deposited films were prepared by exposure of Au substrates to dilute ethanol solutions of the *n*-alkanethiols followed by ethanol rinsing, and vapor-phase-deposited SAMs were prepared by exposure of the Au surface to 10%-of-saturation *n*-alkanethiol vapors followed by $N_2$ purging, which removes loosely bound *n*-alkanethiol molecules from the surface. The matrix of six organic surfaces was studied by FTIR external reflectance spectroscopy (FTIR-ERS), ellipsometry, and cyclic voltammetry, which provide information about the average structure of the SAMs, and a newly developed scanning tunneling microscope (STM)-based method, which provides information about individual SAM defect structures. FTIR-ERS and ellipsometry indicate no detectable differences between liquid- and vapor-phase-deposited SAMs. Data obtained using cyclic voltammetry and STM show that the barrier properties of SAMs depend on the ambient phase from which the SAM assembles, the length of the *n*-alkanethiol, and the chemical nature of the molecular probe used to evaluate the monolayer structure. For example, vapor-phase-deposited Au/$HS(CH_2)_{11}CH_3$ SAMs are better $CN^-$ mass-transfer barriers than their liquid-phase-deposited analogs. However, Au/$HS(CH_2)_{15}CH_3$ SAMs are better $CN^-$ barriers when they are formed from the liquid phase. In contrast, Au/$HS(CH_2)_{11}CH_3$ SAMs prepared from either phase present nearly identical barriers to electron exchange between the Au surface and solution-phase $Ru(NH_3)_6^{3+}$. STM reveals some of the nanostructural details of SAMs and confirms that individual defects govern their barrier properties.

## Introduction

In this article, we contrast structural and chemical properties of self-assembling *n*-alkanethiol monolayers deposited on Au substrates from liquid and vapor phases. This work was prompted by our recent observation that monolayers formed by vapor-phase deposition are qualitatively similar to those prepared in liquid phases.[1-5] Since many organomercaptans have sufficient vapor pressure to yield organic monolayers on Au, we feel it is beneficial to present a more in-depth, quantitative analysis of vapor-phase-deposited monolayers. In this paper, we consider only deposition conditions near room temperature and atmospheric pressure, and therefore our results are intended to complement studies of monolayers formed in ultra-high-vacuum (UHV) and condensed phases.

There are several reasons to consider vapor-phase self-assembly chemistry as an alternative to liquid-phase self-assembly. First, analysis of monolayer structure and chemistry is simplified when measurements are performed in vapor-phase ambients. For example, we recently used mass-sensitive surface acoustic wave (SAW) devices, which do not function in liquid phases, to obtain real-time kinetic measurements of the self-assembly process[1] and subsequent monolayer reaction chemistry.[2-6] Second, solvent effects on monolayers and the substrates on which they form are eliminated in vapor-phase experiments. There are a number of cases when this is important. For example, certain adsorption phenomena, including those based on proton-transfer interactions,[5] generally do not occur in high-dielectric phases. Moreover, it has recently been shown that organomercaptans, as well as thiocyanates and sulfides, dissolve Au in condensed phases during deposition.[7,8] This process may roughen the substrate and compromise the self-assembled monolayer (SAM) barrier properties. It is also likely that solvent molecules can either compete with organomercaptans for binding sites on Au surfaces[9] or become intercalated into such monolayers. Either of these processes decreases the homogeneity, and thus the usefulness, of these important model organic surfaces. Finally, we believe that most technological applications of SAMs will require their formation in the absence of solvents.

Monolayer and multilayer self-assembly chemistry is useful for constructing functional organic surfaces.[3,10-15] A particularly popular and versatile version of monolayer self-assembly occurs when a Au substrate contacts a dilute ethanolic solution of a

* Author to whom correspondence should be addressed.
† Present address: Department of Chemistry, Texas A&M University, College Station, TX 7784-3255.
‡ Present address: Department of Chemistry, University of Minnesota, Minneapolis, MN 55455-0431.
® Abstract published in *Advance ACS Abstracts,* December 1, 1993.
(1) Thomas, R. C; Sun, L.; Crooks, R. M.; Ricco, A. J. *Langmuir* **1991**, *7*, 620.
(2) Sun, L.; Thomas, R. C; Crooks, R. M.; Ricco, A. J. *J. Am. Chem. Soc.* **1991**, *113*, 8550.
(3) Kepley, L. J.; Crooks, R. M.; Ricco A. J. *Anal. Chem.* **1992**, *64*, 3191.
(4) Sun, L.; Kepley, L. J.; Crooks, R. M. *Langmuir* **1992**, *8*, 2101.
(5) Sun, L.; Crooks, R. M.; Ricco, A. J. *Langmuir* **1993**, *9*, 1775.
(6) Xu, C.; Sun, L.; Kepley, L. J.; Crooks, R. M.; Ricco, A. J. *Anal. Chem.* **1993**, *65*, 2102.
(7) , Edinger, K.; Gölzhäuser, A.; Demota, K.; Wöll, Ch.; Grunze, M. *Langmuir* **1993**, *9*, 4–8.
(8) McCarley, R. L.; Kim, Y.-T.; Bard, A. J. *J. Phys. Chem.* **1993**, *97*, 211.
(9) Buttry, D. A., University of Wyoming, personal communication, 1993.
(10) Chailapakul, O.; Crooks, R. M. *Langmuir* **1993**, *9*, 884.
(11) Ross, C. B.; Sun, L.; Crooks, R. M. *Langmuir* **1993**, *9*, 632.
(12) Thomas, R. C.; Houston, J. E.; Michalske, T. A.; Crooks, R. M. *Science* **1993**, *259*, 1883.
(13) Bigelow, W. C.; Pickett, D. L.; Zisman, W. A. *J. Colloid Sci.* **1946**, *1*, 513.
(14) Dubois, L. H.; Nuzzo, R. G. *Annu. Rev. Phys. Chem.* **1992**, *43*, 437 and references therein.
(15) Cao, G.; Hong, H.-G.; Mallouk, T. E. *Acc. Chem. Res.* **1992**, *25*, 420.

0002-7863/93/1515-12459$04.00/0 

suitable organomercaptan.[14,16] This treatment results in surface-adsorbed monolayers possessing well-defined chemical and physical properties, which have been characterized by contact angle measurements, electrochemical methods, FTIR-external reflection spectroscopy (FTIR-ERS), optical ellipsometry, scanning probe microscopy, UHV surface spectroscopy, and other techniques.[14] Except for a few studies,[1-6,17-19] our understanding of organomercaptan monolayers has relied on condensed-phase surface preparation followed *by ex situ* characterization. An excellent summary of these studies recently appeared,[14] but we briefly recount some of the important structural aspects of organomercaptan SAMs here.

Previous results have shown that *n*-alkanethiols spontaneously adsorb to Au from dilute solutions of ethanol and other nonaqueous solvents.[14,16] The resulting monolayer assumes a $(\sqrt{3} \times \sqrt{3})$-*R*30° overlayer structure on Au(111), and it has been shown that adsorption occurs at surface 3-fold hollow sites instead of on the 6-fold symmetric Au surface.[20] Since many Au surfaces have a pronounced (111) texture, the $(\sqrt{3} \times \sqrt{3})R30°$ structure is often assumed to be applicable to all Au substrates, including evaporated films and polycrystalline wires and foils, even when the average Au crystallite diameter is less than 50 nm. The *n*-alkanethiols, which can form nearly crystalline adlayers with coherence lengths on the order of hundreds of nanometers on suitable substrates, are thought to interact with Au according to eq 1. The resulting

$$\text{Au} + \text{SH-R} \rightarrow \text{Au}(\delta^+)/\text{HS}(\delta^-)\text{–R} \qquad (1)$$

$\text{Au}(\delta^+)/\text{HS}(\delta^-)$–R interaction has an energy of about 44 kcal/mol and the SAM is further stabilized by intramonolayer van der Waals interactions.[14] Spectroscopic studies indicate that monolayers are composed of hydrocarbon chains that are tilted about 30° from the surface normal and that SAMs formed from shorter chains are more disordered than those formed from longer-chain molecules: defects are thought to result primarily from gauche conformations within the preferred *all-trans*, extended SAM structure. SAMs are quite robust under normal laboratory conditions, and an additional hydrophobic interaction further increases the stability of methyl-terminated SAMs in aqueous solutions. The best *n*-alkanethiol monolayers contain surprisingly few defect sites, even when prepared on ill-defined substrates.[10,21,22]

We previously showed that approximately monolayer coverages of *n*-alkanethiols spontaneously adsorb to Au surfaces from the vapor phase,[1,2,6] and that such SAMs are qualitatively indistinguishable from those formed by condensed-phase assembly. In this article, we quantitatively contrast some structural and chemical properties of liquid- and vapor-phase-deposited *n*-alkanethiol monolayers formed from $\text{HS}(\text{CH}_2)_n\text{CH}_3$, $n$ = 5, 11, and 15, using FTIR-external reflectance spectroscopy (FTIR-ERS), ellipsometry, scanning tunneling microscopy (STM), and cyclic voltammetry. FTIR-ERS and ellipsometry indicate no detectable differences between liquid- and vapor-phase-deposited SAMs. In contrast, results obtained using cyclic voltammetry and STM suggest that the mass- and electron-transfer barrier properties of SAMs depend on the ambient phase from which the SAM assembles, the length of the *n*-alkanethiol, and the chemical nature of the molecular probe used to evaluate the monolayer structure. For example, vapor-phase-deposited $\text{Au/HS}(\text{CH}_2)_{11}\text{CH}_3$ SAMs are better $\text{CN}^-$ mass-transfer barriers than the corresponding liquid-phase-deposited SAMs, while $\text{Au/HS}(\text{CH}_2)_{15}\text{CH}_3$ SAMs are better $\text{CN}^-$ barriers when they are formed from the liquid phase. In contrast, $\text{Au/HS}(\text{CH}_2)_{11}\text{CH}_3$ SAMs prepared from either phase present nearly identical barriers to electron exchange between the Au surface and solution-phase $\text{Ru}(\text{NH}_3)_6^{3+}$. STM reveals some of the nanostructural details of SAMs and confirms that individual defects govern their barrier properties.

## Experimental Section

**Chemicals.** The following chemicals were obtained from Aldrich and distilled once under reduced pressure prior to use: $\text{CH}_3(\text{CH}_2)_5\text{SH}$, 95%; $\text{CH}_3(\text{CH}_2)_{11}\text{SH}$, 98%; $\text{CH}_3(\text{CH}_2)_{15}\text{SH}$, 98%. All other chemicals were used as received: $\text{CH}_3\text{CH}_2\text{OH}$ (100%, Midwest Grain Products); $\text{H}_2\text{SO}_4$ (98%, J. T. Baker); KCN and $\text{Na}_2\text{HPO}_4$ (Fisher); $\text{Ru}(\text{NH}_3)_6\text{Cl}_3$ (Strem). Water was purified (resistivity ≥18 MΩ-cm) using a Milli-Q reagent water system (Millipore). Other chemicals were of reagent grade purity or better.

**FTIR-ERS.** FTIR-ERS data were acquired using a Digilab FTS-40 spectrometer (Bio-Rad, Cambridge, MA) equipped with a Harrick Scientific "Seagull" reflection accessory and a liquid $\text{N}_2$-cooled MCT detector. All spectra were obtained using *p*-polarized light incident on the substrate at an angle of 84°. All spectra were obtained at 2-$\text{cm}^{-1}$ resolution and are the sum of 256 individual spectra. Minimal baseline correction was applied to all spectra. Substrates were Si(100) wafers coated by thermal evaporation of 100 Å of Cr and 2000 Å of Au. Immediately prior to monolayer modification, Au substrates were cleaned in freshly prepared "piranha" solution (3:1 concentrated $\text{H}_2\text{SO}_4$:30% $\text{H}_2\text{O}_2$; **Caution:** piranha solution reacts violently with organic compounds, and it should not be stored in closed containers) for 15 s, rinsed with deionized water, and then dried in a flowing stream of $\text{N}_2$. Liquid-phase-deposited SAMs were prepared by soaking the clean Au substrates in 1 mM *n*-alkanethiol–ethanol solutions for 4 h, rinsing with ethanol, and then drying in a pure-$\text{N}_2$ stream. A custom-designed flow system was used for preparation of vapor-phase-deposited SAMs.[6] Vapor-phase-deposited monolayers were prepared by passing a 10%-of-saturation *n*-alkanethiol vapor (mixed with $\text{N}_2$) over the substrate for 4 h at a flow rate of 0.5 L/min. Prior to spectral analysis, physisorbed condensates were removed from the substrate by purging with pure $\text{N}_2$ for 1 h at the same flow rate.[1,2,4-6] Since the three *n*-alkanethiols used in this study have different vapor pressures, which have not been reported in the literature, this approach results in different vapor-phase concentrations.

**Ellipsometry.** The substrates prepared for FTIR-ERS measurements were also used for ellipsometric thickness measurements. The method used for determining film thickness has been described previously.[1,2] The value used for the refractive index of the films was 1.45.

**STM.** Au(111) substrates were prepared by melting 0.25-mm-diameter Au wires (99.998%, Johnson-Matthey) in a $\text{H}_2/\text{O}_2$ flame.[23-25] This treatment results in approximately 0.6-mm-diameter spheres that contain a few Au(111) facets on the surface. Immediately prior to monolayer modification, the facets were electrochemically cleaned and polished by scanning their potential 5–10 times between 0.6 and 1.5 V (vs Ag/AgCl, NaCl (3 M)) at 0.02 V/s in an aqueous 0.1 M $\text{HClO}_4$/5 × $10^{-5}$ M HCl solution.[23-26] Following this process the potential was held at 0.6 V for 5 min, which we have found reduces surface roughness, and then the Au ball was removed from the solution at a potential of 0.2 V, which minimizes the surface concentration of adsorbed $\text{Cl}^-$.

The Au balls were modified with SAMs from either the liquid or vapor phase exactly as described previously for the FTIR-ERS experiments. Electrochemical etching was performed in a single-compartment, three-electrode, glass cell containing a Ag/AgCl, NaCl (3 M) reference electrode (Bioanalytical Systems, Inc., West Lafayette, IN) and a Pt counter electrode. Cyanide etching of defects contained within the monolayers was achieved by poising the substrate at a potential of 0.1 V for 30 s in an aqueous electrolyte solution containing 0.1 M KCN and 0.1 M $\text{Na}_2\text{HPO}_4$.[20] Oxygen was not removed from the electrolyte prior to $\text{CN}^-$ etching. All electrochemical experiments were performed using a Pine Instruments Model AFRDE4 bipotentiostat, and data were recorded on a Kipp and Zonen Model BD-90 X–Y recorder.

A NanoScope III STM (Digital Instruments, Santa Barbara, CA) was used for all experiments. Images were obtained using a bias voltage of +300 mV and tip currents in the range of 0.14–0.50 nA (scan rate = 2.00 Hz). Positive bias voltages indicate that electrons tunnel from the STM tip to the Au substrate. Tips were mechanically cut from Pt/Ir (80/20%) wire. As previously described, the STM *z*-piezo was calibrated

(16) Nuzzo, R. G.; Allara, D. L. *J. Am. Chem. Soc.* **1983**, *105*, 4481.
(17) Duevel, R. V.; Corn, R. M. *Anal. Chem.* **1992**, *64*, 337.
(18) Nuzzo, R. G.; Dubois, L. H.; Allara, D. L. *J. Am. Chem. Soc.* **1990**, *112*, 558.
(19) Ong, T. H.; Ward, R. N.; Davies, P. B.; Bain, C. D. *J. Am. Chem. Soc.* **1992**, *114*, 6243.
(20) Sun, L.; Crooks, R. M. *Langmuir* **1993**, *9*, 1951.
(21) Chidsey, C. E. D.; Loiacono, D. N. *Langmuir* **1990**, *6*, 682.
(22) Creager, S. E.; Hockett, L. A.; Rowe, G. K. *Langmuir* **1992**, *8*, 854.
(23) Sun, L.; Crooks, R. M. *J. Electrochem. Soc.* **1991**, *138*, L23.
(24) Hsu, T. *Ultramicroscopy* **1983**, *11*, 167.
(25) Snyder, S. R. *J. Electrochem. Soc.* **1992**, *139*, 5C.
(26) Trevor, D. J.; Chidsey, C. E. D.; Loiacono, D. N. *Phys. Rev. Lett.* **1989**, *62*, 929.

by measuring several independently prepared Au(111) monoatomic step edges and correlating the mean experimental value to the theoretical Au(111) interlayer spacing of 0.235 nm.[20] To minimize the extent to which the SAMs are altered by the tip,[11] all of the STM data presented in this paper were obtained during the first three scans in a particular region of the substrate.

**Cyclic Voltammetry.** Substrates used for cyclic voltammetric analyses were Au balls prepared identically to those used for STM experiments except that the entire ball, with the exception of a single Au(111) facet, was covered with silicone rubber (Dow-Corning, Catalog No. 698).[11] Immediately prior to monolayer adsorption the exposed facet was electrochemically cleaned and polished as described for the STM experiments. SAM modification of the substrate was performed identically to that described for FTIR-ERS, ellipsometry, and STM experiments. Electrochemical experiments were carried out in a cell configured identically to that described for the $CN^-$ etching experiments.

## Results and Discussion

**FTIR-ERS.** Fourier transform infrared external reflection spectroscopy (FTIR-ERS) has been used extensively for characterizing *n*-alkanethiol SAMs. In this single-reflection spectroscopic technique, the extent of IR absorption depends on the number of surface dipoles, their transition dipole moments, and their average orientation relative to the local surface normal direction.[27,28] It is possible to extract highly detailed information about the average physical and chemical environment of *n*-alkanethiol SAMs from an analysis of the C–H stretching region of FTIR-ERS spectra.[14,18,29-31] On the basis of the C–H stretching peak positions and shapes it has been inferred that long-chain *n*-alkanethiol SAMs prepared from ethanol solutions reside in a close-packed crystalline-like environment. Short-chain *n*-alkanethiols that contain less than about 10 carbon atoms result in more liquid-like surface phases because of decreased intramonolayer van der Waals interactions. Terminal groups can also exert a strong influence over the degree of ordering in SAMs.[21]

We prepared SAMs on polycrystalline Au surfaces using both liquid- and vapor-phase-deposition techniques, and then we evaluated the resulting organic surfaces using FTIR-ERS. Figure 1 shows FTIR-ERS data obtained in the C–H stretching region for SAMs prepared from $HS(CH_2)_nCH_3$, $n$ = 5, 11, and 15. For each of the three *n*-alkanethiols, spectra are shown for SAMs prepared by (1) liquid-phase deposition, (2) vapor-phase deposition before ethanol rinsing, and (3) vapor-phase deposition after ethanol rinsing. We collected spectra before and after ethanol rinsing to evaluate the effect of solvent contact with vapor-phase-deposited SAMs.

SAMs of $Au/HS(CH_2)_5CH_3$ prepared by either liquid- or vapor-phase deposition yield poorly-defined spectroscopic features in the C–H stretching region (Figure 1, a–c). Moreover, the spectra are difficult to reproduce, which indicates the monolayers are disordered and have variable surface coverages. We obtained better-defined and fully-reproducible spectra for $Au/HS(CH_2)_{11}CH_3$ (Figure 1d–f) and $Au/HS(CH_2)_{15}CH_3$ SAMs (Figure 1g–i) deposited from either the liquid or vapor phase. For example, the liquid-phase-deposited $Au/HS(CH_2)_{15}CH_3$ SAM results in spectra that consist of 5 well-defined peaks at 2965 $cm^{-1}$ ($CH_3$ asymmetric in-plane C–H stretching: $\nu_{a,ip,CH_3}$), 2938 $cm^{-1}$ ($CH_3$ symmetric Fermi-resonance-enhanced C–H stretching: $\nu_{s,FR,CH_3}$), 2919 $cm^{-1}$ ($CH_2$ asymmetric C–H stretching: $\nu_{a,CH_2}$), 2878 $cm^{-1}$ ($CH_3$ symmetric Fermi-resonance-enhanced C–H stretching: $\nu_{s,FR,CH_3}$), and 2850 $cm^{-1}$ ($CH_2$ symmetric C–H stretching: $\nu_{s,CH_2}$).[18] Table I lists peak positions that correspond to Figure 1d–i and provides a comparison with the frequencies of bulk-phase liquid and solid $HS(CH_2)_{11}CH_3$ and $HS(CH_2)_{15}CH_3$. Table I also lists the peak intensities and full-widths at half-maximum (fwhm) for the $\nu_{s,CH_2}$ and $\nu_{a,ip,CH_3}$ bands, which we selected for analysis because they are well-resolved.

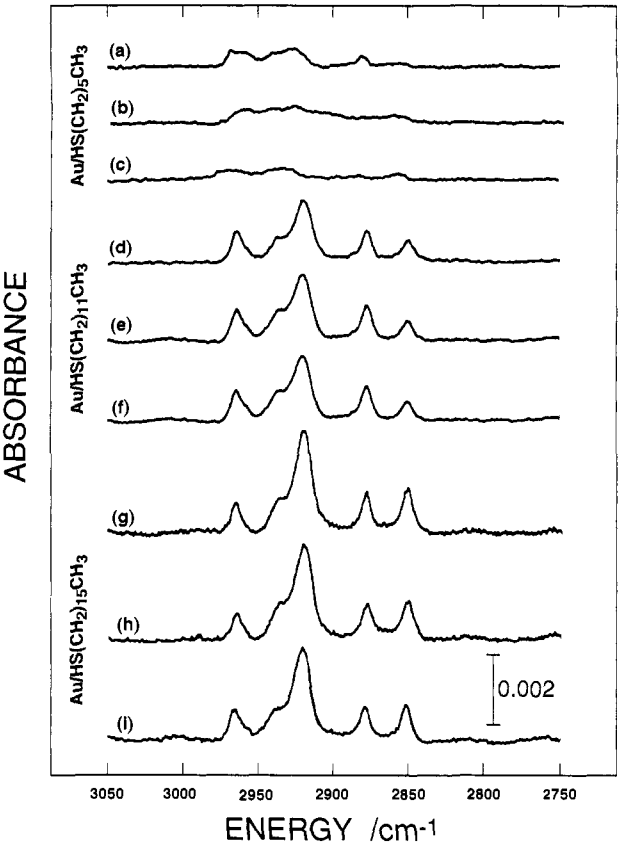


**Figure 1.** FTIR spectra of liquid- and vapor-phase-deposited *n*-alkanethiol SAMs on Au surfaces: (a) $Au/HS(CH_2)_5CH_3$, liquid; (b) $Au/HS(CH_2)_5CH_3$, vapor; (c) $Au/HS(CH_2)_5CH_3$, vapor after rinsing with ethanol; (d) $Au/HS(CH_2)_{11}CH_3$, liquid; (e) $Au/HS(CH_2)_{11}CH_3$, vapor; (f) $Au/HS(CH_2)_{11}CH_3$, vapor after rinsing with ethanol; (g) $Au/HS(CH_2)_{15}CH_3$, liquid; (h) $Au/HS(CH_2)_{15}CH_3$, vapor; (i) $Au/HS(CH_2)_{15}CH_3$, vapor after rinsing with ethanol.

The peak positions and fwhm given in Table I indicate that the methylene chains of vapor-phase-deposited monolayers are in an environment that is indistinguishable from liquid-phase-deposited SAMs. That is, FTIR-ERS indicates that SAMs deposited from the vapor phase consist primarily of extended, *all-trans* conformers in a crystalline-like environment. The $\nu_{a,ip,CH_3}$ peak intensities for $Au/HS(CH_2)_{11}CH_3$ and $Au/HS(CH_2)_{15}CH_3$ SAMs deposited from liquid and vapor phases are identical within the limits of our experimental error, which strongly suggest that the method of deposition does not change the SAM surface coverage density or molecular tilt angle. In contrast, the peak intensities for $\nu_{s,CH_2}$ show a significant dependence on chain length, but not on the method of deposition.

The FTIR-ERS data indicate that *n*-alkanethiol SAMs self-assemble from vapor-phase ambients in much the same way as they do from liquid phases. Some subtle differences in the surface coverage, orientation, and number and nature of defects with SAMs may exist (*vide infra*), but FTIR-ERS is not sufficiently sensitive to resolve them. We also compared FTIR-ERS data for vapor-phase-deposited monolayers before (Figure 1b,e,h) and after (Figure 1c,f,i) ethanol rinsing, but we did not observe any significant differences (Table I). This indicates that the stability of the liquid- and vapor-phase-deposited films is also quite similar.

To summarize, the FTIR-ERS results indicate the following: (1) spectra of *n*-alkanethiol SAMs formed by vapor-phase self-assembly are indistinguishable from spectra of liquid-phase-deposited SAMs; (2) FTIR-ERS spectra of long-chain vapor-phase-deposited films are highly reproducible and indistinguishable from SAMs formed from liquid phases; (3) the structure and stability of vapor-phase-deposited *n*-alkanethiol SAMs are a

(27) Greenler, R. G. *J. Chem. Phys.* **1966**, *44*, 310.
(28) Porter, M. D. *Anal. Chem.* **1988**, *60*, 1143A.
(29) Allara, D. L.; Swalen, J. D. *J. Phys. Chem.* **1982**, *86*, 2700.
(30) Porter, M. D.; Bright, T. B.; Allara, D. L.; Chidsey, C. E. D. *J. Am. Chem. Soc.* **1987**, *109*, 3559.
(31) Laibinis, P.; Whitesides, G. M.; Allara, D. L.; Tao, Y.-T.; Parikh, A. N.; Nuzzo, R. G. *J. Am. Chem. Soc.* **1991**, *113*, 7152.

**Table I.** Peak Positions, Absorbances, and Full-Widths at Half-Maximum (fwhm) for the C–H Stretching Modes of $CH_3(CH_2)_{11}SH$ and $CH_3(CH_2)_{15}SH$ in Bulk Crystalline and Liquid Phases and SAMS on Polycrystalline Au Surfaces

| | | | | $Au/HS(CH_2)_{11}CH_3$ | | | $Au/HS(CH_2)_{15}CH_3$ | | |
|---|---|---|---|---|---|---|---|---|---|
| | | | | vapor phase | | | vapor phase | | |
| vibrational mode | | crystalline state[a] | liquid state[a] | before rinse | after rinse | liquid phase | before rinse | after rinse | liquid phase |
| $\nu_{a,ip,CH_3}$ | peak position/$cm^{-1}$ | *b* | *b* | 2965 | 2965 | 2966 | 2966 | 2965 | 2965 |
| | peak intensity/$10^{-3}$ | | | 0.8 ± 0.1 | 0.8 ± 0.1 | 0.8 ± 0.1 | 0.8 ± 0.1 | 0.8 ± 0.1 | 0.8 ± 0.1 |
| | fwhm/$cm^{-1}$ | | | 11 ± 1 | 11 ± 1 | 10 ± 1 | 10 ± 1 | 10 ± 1 | 9 ± 1 |
| $\nu_{s,FR,CH_3}$ | peak position/$cm^{-1}$ | *b* | *b* | 2937 | 2938 | 2938 | 2938 | 2939 | 2938 |
| $\nu_{a,CH_2}$ | peak position/$cm^{-1}$ | 2918 | 2924 | 2921 | 2921 | 2921 | 2920 | 2919 | 2919 |
| $\nu_{s,FR,CH_3}$ | peak position/$cm^{-1}$ | *b* | *b* | 2878 | 2878 | 2879 | 2879 | 2879 | 2878 |
| $\nu_{s,CH_2}$ | peak position/$cm^{-1}$ | 2851 | 2855 | 2851 | 2851 | 2851 | 2851 | 2851 | 2850 |
| | peak intensity/$10^{-3}$ | | | 0.5 ± 0.1 | 0.5 ± 0.1 | 0.5 ± 0.1 | 1.1 ± 0.2 | 1.1 ± 0.2 | 1.2 ± 0.2 |
| | fwhm/$cm^{-1}$ | | | 9 ± 1 | 10 ± 1 | 10 ± 1 | 9 ± 1 | 9 ± 1 | 9 ± 1 |

[a] From ref 30. [b] These bands are not fully resolved.

**Table II.** Ellipsometrically-Measured Film Thicknesses (Å) of SAMs Formed by Liquid- and Vapor-Phase Deposition

| | Au/ $HS(CH_2)_5CH_3$ | Au/ $HS(CH_2)_{11}CH_3$ | Au/ $HS(CH_2)_{15}CH_3$ |
|---|---|---|---|
| liquid phase | 2.5 ± 1.9 | 11.3 ± 2.2 | 18.5 ± 2.1 |
| vapor phase | 3.9 ± 1.5 | 11.2 ± 0.5 | 20.6 ± 3.0 |

function of the chain length, just as they are for liquid-phase-deposited SAMs (shorter chains yield less-ordered monolayers with lower surface coverage densities); and (4) immersion of vapor-phase-deposited SAMs of $HS(CH_2)_{11}CH_3$ and $HS(CH_2)_{15}CH_3$ into ethanol or prolonged exposure to the laboratory ambient have no detectable effect on the monolayers.

In considering these conclusions, two aspects of the experimental method must be emphasized. First, FTIR-ERS is only useful for determining the average characteristics of SAMs, and it is not sufficiently sensitive to detect subtle changes in the film structure or major differences in small regions of the structure. To better understand these subtle differences we rely on the electrochemical and STM methods discussed later. Second, we have picked a particular protocol for forming SAMs from vapor-phase ambients on the basis of a series of control experiments. FTIR-ERS, ellipsometry, and STM data indicate that under the pressure, temperature, and vapor concentration conditions used in these studies, the structure of vapor-phase-deposited SAMs ceases to change after 4 h of exposure to the *n*-alkanethiol and a subsequent 1-h pure-$N_2$ purge.[1] However, shorter deposition and purge times may result in SAMs with different properties. We have not fully investigated the effect of *n*-alkanethiol partial pressure on SAM structures, but we have reason to believe that partial pressures near saturation can lead to stable, multilayer SAMs.[1] It is also possible that post-deposition treatments, such as thermal annealing, will affect the SAM structure.

**Ellipsometry.** We used optical ellipsometry to determine the thicknesses of liquid- and vapor-phase-deposited SAMs (Table II). Ellipsometry, like FTIR-ERS, measures the average thickness of SAMs with millimeter-scale lateral resolution, but it does not provide any information about molecular-scale structural details. Moreover, there is some question about the accuracy of ellipsometrically-determined thicknesses of monolayer-thick SAMs, since it is necessary to postulate the index of refraction of the SAM and ensure that both the Au control surface and the SAM surface are free from impurities. These problems have led to a significant degree of variability in ellipsometrically-determined film thicknesses for SAMs that were prepared virtually identically.[30,32] Regardless of these problems with absolute thickness determinations, ellipsometric measurements obtained using the same instrument, in the same laboratory, and on the same day are useful for comparison purposes.

We measured film thicknesses in two different locations on each of the substrates used to obtain the FTIR-ERS data discussed previously. The results obtained for the liquid-phase-deposited SAMs are comparable to results that have been reported by others,[32] and the thickness values we obtained for vapor-phase-deposited SAMs are identical to these values within the experimental accuracy of our measurements. We conclude that approximately one monolayer of each SAM deposits onto the Au substrates from either the liquid or vapor phase, in accord with the FTIR-ERS results. However, neither FTIR-ERS nor ellipsometry are sufficiently sensitive to detect subtle difference in SAM structures.

**Scanning Tunneling Microscopy.** Scanning tunneling microscopy (STM) has been used previously to obtain near-atomic-resolution images of *n*-alkanethiol SAMs on atomically flat Au surfaces,[33] but the interpretation of these data remain uncertain.[34] STM images of SAMs that have been acquired at lower resolution reveal small cylindrical features that range from 2 to 5 nm in diameter.[7,11,20,35] We will refer to these features as pits since they appear as depressions in STM images. Until recently, we believed these pits were best described by one or both of the following models. The molecular-defect model postulates that the pits correspond to regions in which *n*-alkanethiol molecules may be absent or loosely packed.[11,20,35a] In this model, differences in tunneling current are brought about by differences in the work function of the Au surface or differences in tunneling probability that arise from different SAM packing arrangements. The Au-dissolution model postulates that the pits are due to topographical changes in the Au substrate brought about by thiol-induced dissolution of Au.[7,35b] In this section, we will show that neither of these models is correct, and we will contrast the nanostructure of SAMs formed from both ethanol solutions and from the vapor phase. Specifically, we will compare the apparent defect densities contained within SAMs constructed from *n*-alkanethiols of varying length as a function of the ambient from which the monolayers self-assemble.

We recently developed a method that combines electrochemical $CN^-$ etching and STM to yield insight into the nanostructural properties of SAMs.[20] We use this method here to enlarge only those adventitious SAM defects that are of the correct chemical and structural configuration to admit $CN^-$. This element of molecular specificity, which relies on electrochemical selectivity, enhances the inherently weak molecular specificity of STM. The details of the experiment are described in the experimental section, but briefly, we etched the SAM-coated Au substrates at 0.1 V for 30 s in an aqueous 0.1 M KCN solution.

Figures 2–4 are representative STM images of *n*-alkanethiol SAMs. The images on the left side of each figure were obtained from liquid-phase-deposited SAMs, and the images on the right

(32) Bain, C. D.; Troughton, E. B.; Tao, Y.-T.; Evall, J.; Whitesides, G. M.; Nuzzo, R. G. *J. Am. Chem. Soc.* **1989**, *111*, 321.

(33) Widrig, C. A.; Alves, C. A.; Porter, M. D. *J. Am. Chem. Soc.* **1991**, *113*, 2805.

(34) Kim, Y.-T.; McCarley, R. L.; Bard, A. J. *J. Phys. Chem.* **1992**, *96*, 7416.

(35) (a) Kim, Y.-T.; Bard, A. J. *Langmuir* **1992**, *8*, 1096. (b) Häussling, L.; Michel, B.; Ringsdorf, H.; Rohrer, H. *Angew. Chem., Int. Ed. Engl.* **1991**, *30*, 569.

**Table III.** Fractional Extent of Etching of SAM-Modified Au Surfaces in $CN^-$ Solutions

| | liquid-phase deposition | vapor-phase deposition |
|---|---|---|
| $Au/HS(CH_2)_5CH_3$ | 1 | 1 |
| $Au/HS(CH_2)_{11}CH_3$ | 0.29 ± 0.04 | 0.05 ± 0.04 |
| $Au/HS(CH_2)_{15}CH_3$ | 0.0002 ± 0.0001 | 0.004 ± 0.003 |

side were obtained from vapor-phase-deposited SAMs. Images acquired before $CN^-$ etching are shown on the top of each of these figures and the after-etching results are shown on the bottom.

To quantitatively compare the nanostructure of vapor- and liquid-phase-deposited SAMs, we must quantify the extent to which each SAM prevents $CN^-$ attack on the underlying Au substrate; there are two approaches to this problem. Either we can count the number density of $CN^-$-developed etch pits, or we can estimate the total fraction of the Au surface that is etched by $CN^-$. We have used the latter approach because the pits begin to merge after extensive etching, which makes counting ambiguous. As discussed later in this section, only those pits that permit $CN^-$ penetration, which is a relatively small fraction, are electrochemically etched. We are able to distinguish between etched and unetched pits by measuring their depth: after etching the pits become significantly deeper. Table III shows the average fraction of the surface that was etched for several SAM-modified substrates that were prepared identically to those shown in Figures 2–4. From Table III it is apparent that SAMs prepared from long-chain *n*-alkanethiols block $CN^-$ dissolution of Au more effectively than SAMs formed from shorter-chain *n*-alkanethiols, which is in agreement with results obtained by others using purely electrochemical methods.[14,22,30] Moreover, this trend is observed regardless of whether SAMs are deposited from liquid or vapor phases. Table III also reveals that the absolute degree to which SAMs block trans-monolayer mass transport of $CN^-$ depends not only on the thickness of the SAM but also on the ambient phase from which the SAM self-assembles.

We now compare the nanostructure of SAMs formed from liquid and vapor phases in detail. The images in Figure 2 were obtained for $Au/HS(CH_2)_{11}CH_3$ SAMs prepared from liquid and vapor phases before and after $CN^-$ etching. For $Au/HS(CH_2)_{11}CH_3$ SAMs prepared from ethanol solutions (Figure 2a), we observe monodispersed pits that range in diameter from 2 to 5 nm. $Au/HS(CH_2)_{11}CH_3$ SAMs prepared from the vapor phase (Figure 2c) also contain 2–5-nm-diameter pits, but the dominant features are significantly larger features with diameters in the range 5–10 nm. No pit-like features are present on the Au surfaces prior to SAM modification, and STM images of vapor-phase-deposited SAMs do not change after extensive rinsing with ethanol. We found that the depth of the smaller pits depends strongly on the sharpness of the Pt/Ir STM tip. However, the depth of the larger pits, which is about the same as the height of one Au(111) step,[20] shows only a weak tip-shape dependence.

If we assume that the 2–5-nm-diameter pits present within liquid-phase-deposited SAMs result from thiol-induced substrate dissolution, then the formation of pits on vapor-phase-deposited SAMs is surprising since we would not expect the $Au(\delta^+)/HS(\delta^-)$–R complexes to have sufficient vapor pressure to escape from the substrate surface.[36] However, if we assume that the molecular-defect model is correct, then the vapor-phase-deposited $Au/HS(CH_2)_{11}CH_3$ SAMs should offer less resistance to $CN^-$ etching than SAMs deposited from solution since there are so many large (5–10 nm) pits present. This prediction is contrary to our experimental observations, which are typified by the images of $Au/HS(CH_2)_{11}CH_3$ SAMs after $CN^-$ etching shown in parts b and d of Figure 2 and the data presented in Table III. These data reveal that about 60 times more of the liquid-phase-deposited SAMs is etched compared to the vapor-phase-deposited SAMs.

(36) Tarlov, M. J.; Newman, J. G. *Langmuir* **1992**, *8*, 1398.
(37) Schott, J. H.; White, H. S. *Langmuir* **1992**, *8*, 1955.

Interestingly, we observe that more than half of the large 5–10-nm-diameter pits on the vapor-phase-deposited SAM surfaces remain unchanged after electrochemical $CN^-$ etching. This result and the observation that many of these pits appear triangular (Figure 2c,d)[20] strongly suggest that these apparent defects are not pits that penetrate through the SAMs, but rather depressions in the Au(111) surface itself. At the present time we do not fully understand the presence of either the 2–5-nm-diameter pits, which appear on both the vapor- and liquid-phase-deposited SAMs, or the 5–10-nm-diameter pits that often appear triangular, which are observed exclusively on the vapor-phase-deposited SAMs, but we are certain that neither the Au-dissolution model nor the molecular-defect model correctly accounts for the presence of the pits. It is clear, however, that $Au/HS(CH_2)_{11}CH_3$ SAMs deposited from the vapor phase permit far less contact of solution-phase $CN^-$ with the underlying Au surface, and therefore these SAMs are better mass-transfer barriers under the conditions used in this experiment.

As shown in Figure 3, $Au/HS(CH_2)_{15}CH_3$ SAMs formed from either the liquid or vapor phase exhibit surface morphology and electrochemical etching behavior that is very similar to that just described for $Au/HS(CH_2)_{11}CH_3$ SAMs. For example, prior to $CN^-$ etching, the liquid-phase-deposited $Au/HS(CH_2)_{15}CH_3$ SAMs contain monodispersed pits ranging from 2 to 5 nm in diameter (Figure 3a), while the SAMs prepared from the vapor phase contain both small and large pits (Figures 3c). The number density of pits present on the vapor-phase-deposited $Au/HS(CH_2)_{15}CH_3$ and $Au/HS(CH_2)_{11}CH_3$ SAM surfaces is about the same, and the number density of pits in the two liquid-phase-deposited SAMs is also about the same.

After $CN^-$ etching, $Au/HS(CH_2)_{15}CH_3$ SAMs contain fewer etch pits than $Au/HS(CH_2)_{11}CH_3$ SAMs regardless of whether they are deposited from the liquid or vapor phase; however, the liquid- and vapor-phase-deposited $Au/HS(CH_2)_{15}CH_3$ SAMs exhibit a very different resistance to $CN^-$ penetration (Figure 3b,d, Table III). In contrast to the results obtained for $Au/HS(CH_2)_{11}CH_3$ SAMs, the liquid-phase-deposited $Au/HS(CH_2)_{15}CH_3$ SAMs are much more resistant to $CN^-$ penetration than the vapor-phase-deposited $Au/HS(CH_2)_{15}CH_3$ SAMs. This result indicates that the number density of small cylindrical pits determined prior to $CN^-$ etching, which is about the same in Figures 2a, 2c, 3a, and 3c, does not reliably reflect the true number of monolayer defects that permit ion penetration: whatever their origin, these pits have little correspondence to SAM barrier properties. It also suggests that the pits present within the monolayers prepared from the liquid phase may arise from the same phenomena that lead to the somewhat larger, and equally electroinactive, pits present within the SAMs prepared from the vapor phase (Figures 2c and 3c).

The $Au/HS(CH_2)_5CH_3$ SAMs prepared from either the liquid or vapor phase also contain 2–5-nm-diameter pits prior to $CN^-$ etching (Figure 4). In contrast to the longer-chain SAMs, neither liquid- nor vapor-phase-deposited $Au/HS(CH_2)_5CH_3$ SAMs passivate the Au surface, and we observe severe roughening of these substrates when they are electrochemically etched in $CN^-$. However, the Au surface covered with the vapor-phase-deposited $Au/HS(CH_2)_5CH_3$ SAM is less disrupted than the surface covered with the liquid-phase-deposited SAM. For example, we sometimes observe step edges on the surfaces covered with vapor-phase-deposited SAMs (Figure 4d), but we never observe crystallographic features on the liquid-phase-deposited $Au/HS(CH_2)_5CH_3$ SAMs (Figure 4b). Thus, we conclude that the vapor-phase-deposited $Au/HS(CH_2)_5CH_3$ SAMs are somewhat better mass-transfer barriers than their liquid-phase-deposited counterparts.

To summarize, the STM data complement and are consistent with results obtained by FTIR-ERS. FTIR-ERS data provide information about the average structure of SAMs on a millimeter- to centimeter-resolution scale, while this STM method provides information on a nanometer- to micron-resolution scale. The

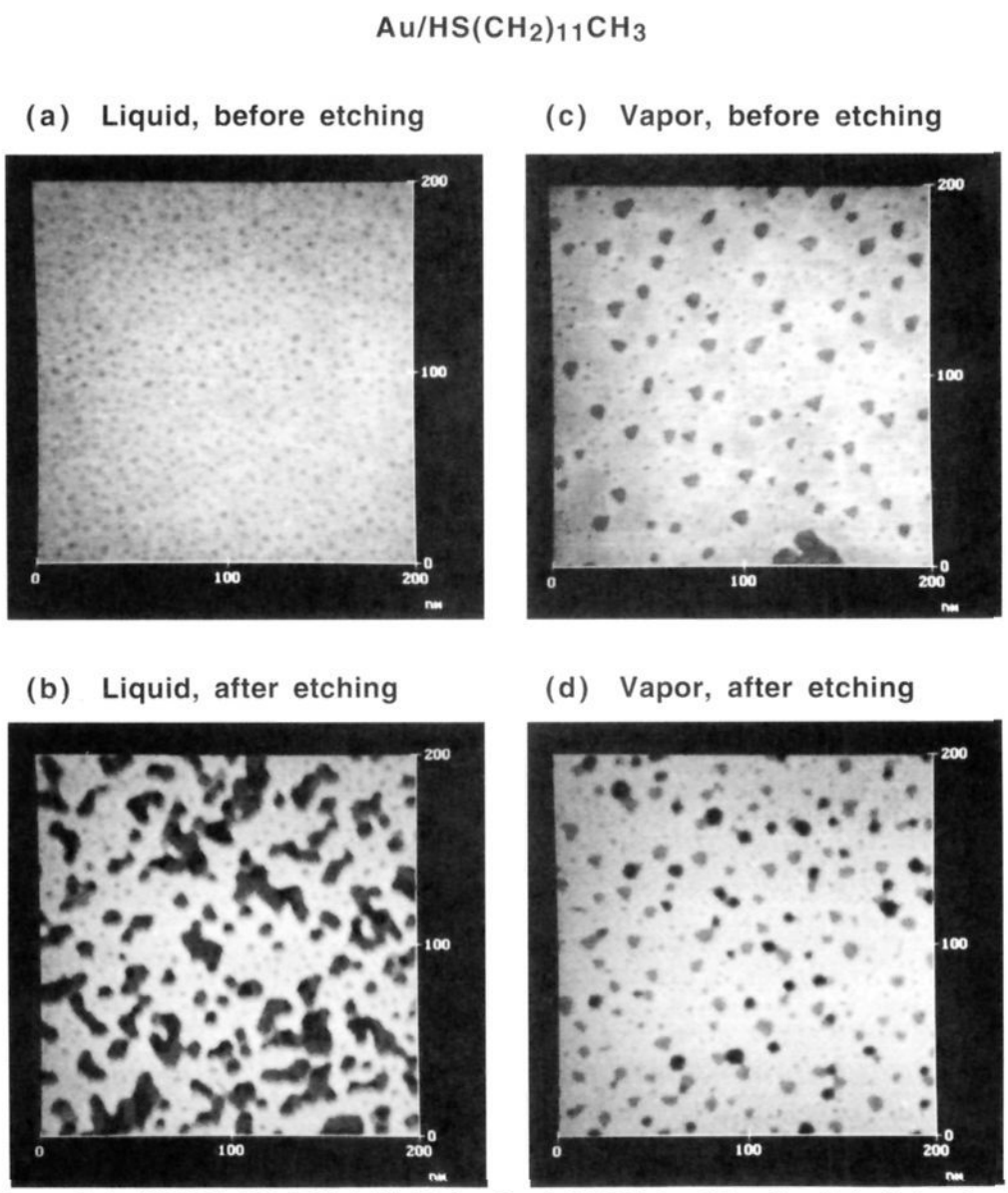


**Figure 2.** STM images of a $Au/HS(CH_2)_{11}CH_3$ SAM: (a) liquid-phase-deposited SAM before $CN^-$ etching; (b) liquid-phase-deposited SAM after $CN^-$ etching; (c) vapor-phase-deposited SAM before $CN^-$ etching; (d) vapor-phase-deposited SAM after $CN^-$ etching. All images represent a 200 nm × 200 nm field and the full gray scale for all images is 4 nm.

following trends can be extracted from the STM results shown in Figures 2–4 and Table III. First, liquid-phase-deposited SAMs always contain monodispersed pits that range in diameter from 2 to 5 nm that we have never detected on the substrate prior to SAM modification. Vapor-phase-deposited SAMs contain two different kinds of pits: the first appear identical to those found within the liquid-phase-deposited SAMs, while the second type is somewhat larger. Prior to $CN^-$ etching, the number density of pits within the SAMs is about the same regardless of its thickness or whether it was deposited from the liquid or vapor phase. This observation suggests that pit formation is governed more by the substrate, or perhaps the $Au(\delta^+)/HS(\delta^-)$–R interaction, than by the solvent, or the length or extent of ordering of the *n*-alkanethiols. The observation that pits appear within SAMs that are deposited from the vapor phase clearly indicates that the Au-dissolution model is incorrect. Since the pit structures are different on the liquid- and vapor-deposited surfaces, it is not likely that the STM tip itself induces pit formation.

Second, we find that there is no clear correlation between either the number of pits or their size prior to electrochemical etching and the extent to which $CN^-$ can penetrate to the surface. This means the pits do not result from the absence of *n*-alkanethiol molecules, which provides additional evidence that the pits are not induced by the STM tip, and that the molecular-defect model does not correctly describe pit formation. Third, we find the combination of electrochemical $CN^-$ etching and STM reveals true defects in the SAMs, and that for deposition from a particular ambient phase there are more real defects in the shorter SAMs than in the longer SAMs. Fourth, the shorter-chain, vapor-phase-deposited SAMs result in better mass transfer barriers than liquid-phase-deposited SAMs, but $Au/HS(CH_2)_{15}CH_3$ SAMs exhibit the opposite behavior. This result probably suggests that solvent interferes with self-assembly of the shorter *n*-alkanethiols, possibly through loose incorporation into the SAM, but that solvent assists in the assembly of longer-chain *n*-alkanethiols by allowing more flexural freedom of the hydrocarbon tail groups. That is, in $Au/HS(CH_2)_{15}CH_3$ SAMs the deleterious effects of solvent incorporation are overcome by the higher degree of structural freedom afforded by solvation.

Finally, we come to the question of the origin of the small cylindrical pits that are apparent in all the pre-etched SAM monolayers we have imaged. We now believe that these features result from thiol-stimulated movement of Au atoms resident near the substrate surface, and that their presence is not a strong

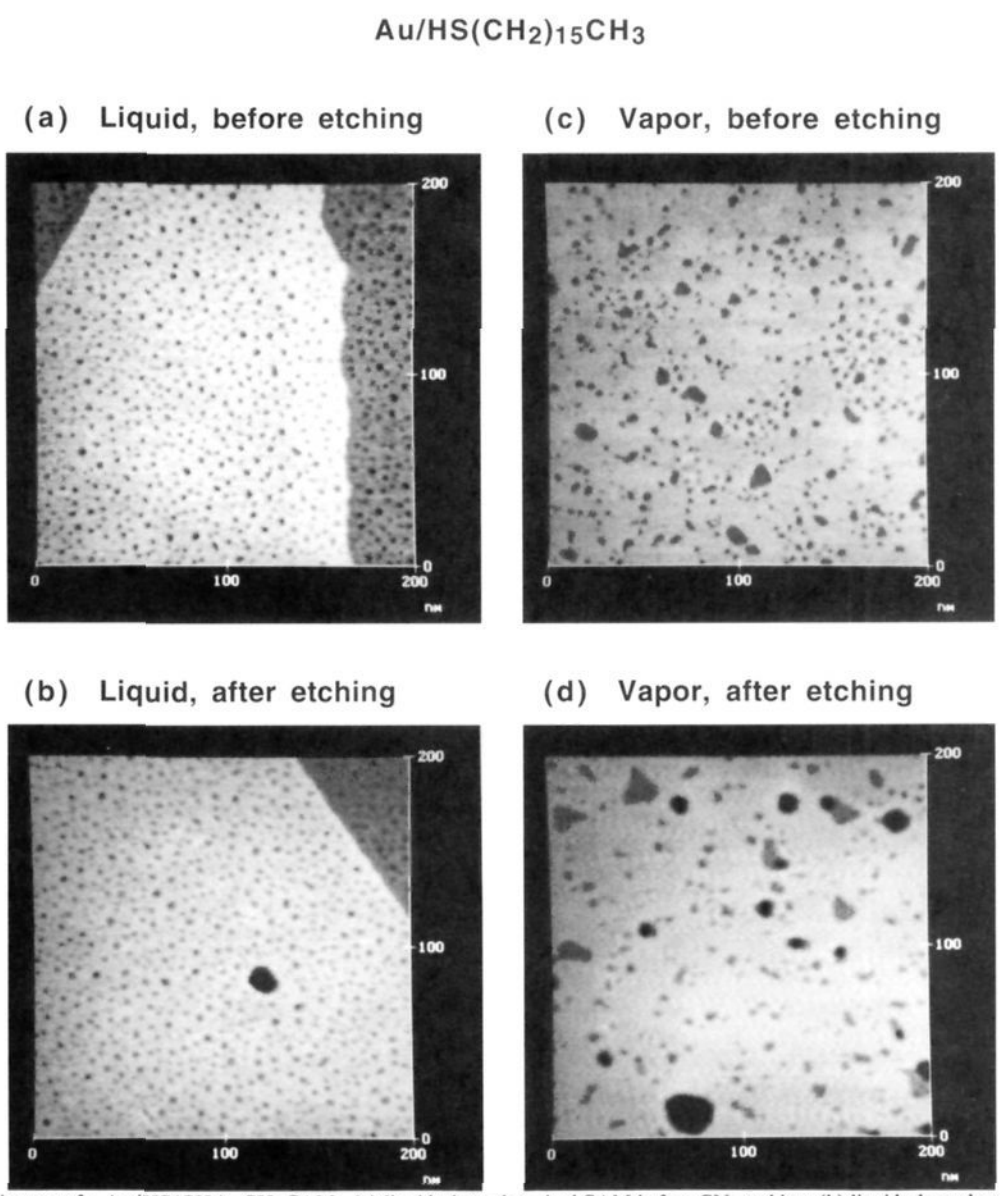


**Figure 3.** STM images of a $Au/HS(CH_2)_{15}CH_3$ SAM: (a) liquid-phase-deposited SAM before $CN^-$ etching; (b) liquid-phase-deposited SAM after $CN^-$ etching; (c) vapor-phase-deposited SAM before $CN^-$ etching; (d) vapor-phase-deposited SAM after $CN^-$ etching. All images represent a 200 nm × 200 nm field and the full gray scale for all images is 4 nm.

function of the ambient phase from which the SAMs form. While we are uncertain about the nature of the energetics that might drive pit formation, it may result from a thiol-induced surface restructuring that changes the Au atom surface density. There is precedent for this speculation: Schott and White found that an STM tip can be used to induce a $1 \times 1$ to $\sqrt{3} \times 22$ surface reconstruction on Au(111).[37] This reconstruction increases the surface atom density by about 5%, and pits, which are similar to those we have observed, form near the reconstructed surface. Presumably the atoms necessary for the reconstruction originated in the pits. In the absence of supporting data, however, we believe that additional speculation on this issue is not warranted at the present time.

**Cyclic Voltammetry.** We have used cyclic voltammetry to contrast the barrier properties of liquid- and vapor-phase-deposited SAMs. In this experiment, a SAM-coated Au substrate is immersed in an electrolyte solution containing redox-active probe molecules. Depending on the size and chemical nature of the probe molecules and the nanoscopic structure of the SAM, the probe molecules may completely or partially penetrate the SAM and undergo electron transfer with the Au substrate. Three possible modes of interaction are possible. First, if there are many defects within the SAM that permit probe molecules to exchange electrons with the underlying substrate, then the resulting cyclic voltammetric response will appear peak-shaped.[30] This is a consequence of linear diffusion of the probe molecule to the substrate. Second, if there is a low density of micron- or nanometer-scale defects, then each defect will behave as a single ultramicroelectrode.[10,38,39] Diffusion to individual electrodes will be radial, and as long as they are spaced sufficiently far apart that their diffusion layers do not overlap, the resulting cyclic voltammetric response will appear plateau shaped.[10] Third, if there are no defect sites through which probe molecules can completely or partially penetrate, their average point of closest approach to the electrode will be roughly defined by the average thickness of the monolayer.[40-42] In this case it may be possible to observe very small tunneling currents between the substrate and probe, which will result in cyclic voltammograms characterized by exponential shapes.

(38) Sabatani, E.; Rubinstein, I. *J. Phys. Chem.* **1987**, *91*, 6663.
(39) Bilewicz, R.; Majda, M. *J. Am. Chem. Soc.* **1991**, *113*, 5464.
(40) Chidsey, C. E. D. *Science* **1991**, *251*, 919.
(41) Becka, A. M.; Miller, C. J. *J. Phys. Chem.* **1992**, *96*, 2657.
(42) Finklea, H. O.; Hanshew, D. D. *J. Am. Chem. Soc.* **1992**, *114*, 3173.

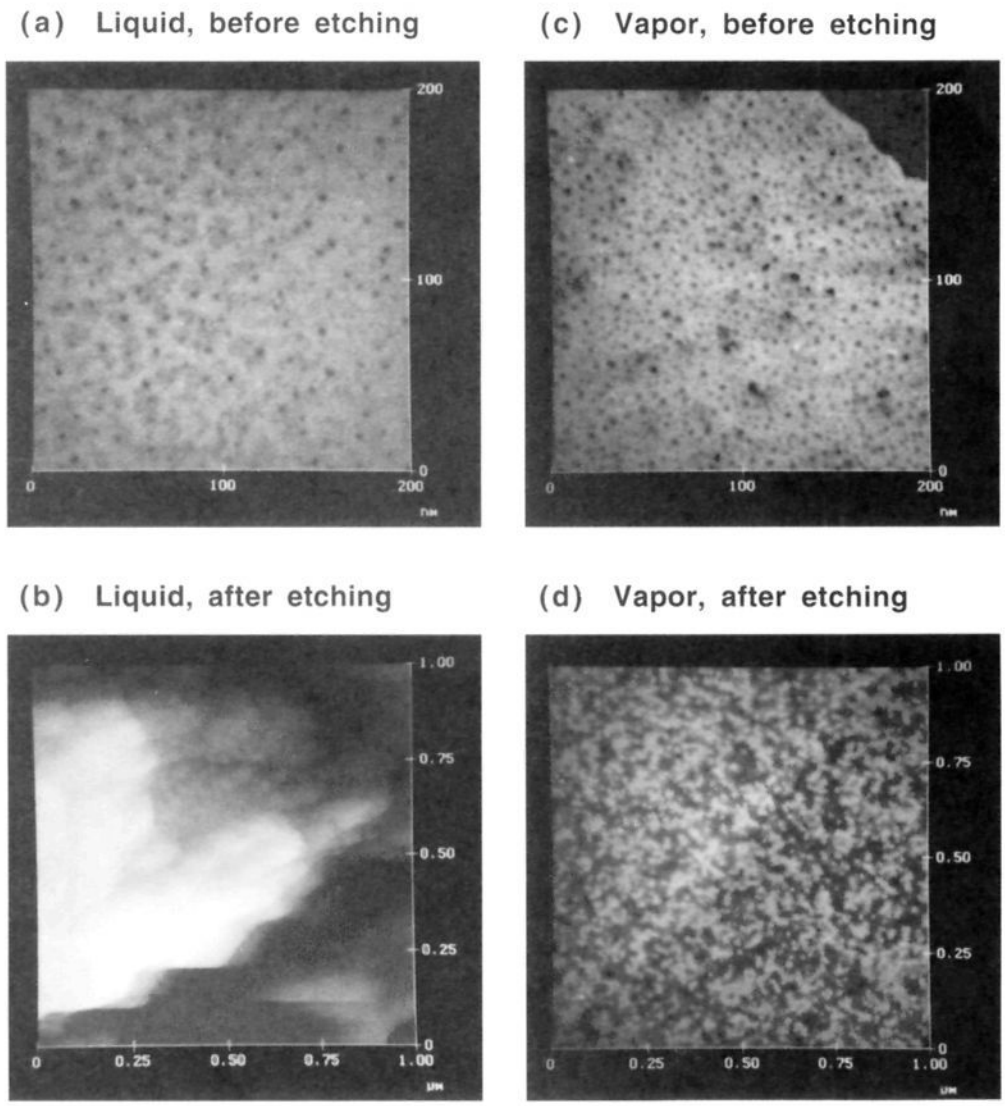


**Figure 4.** STM images of a $Au/HS(CH_2)_5CH_3$ SAM: (a) liquid-phase-deposited SAM before $CN^-$ etching; (b) liquid-phase-deposited SAM after $CN^-$ etching; (c) vapor-phase-deposited SAM before $CN^-$ etching; (d) vapor-phase-deposited SAM after $CN^-$ etching. Images a and c represent a 200 nm × 200 nm field, images b and d represent a 1 μm × 1 μm field, and the full gray scale for all images is 4 nm.

Interpretation of results from cyclic voltammetric experiments is most straightforward for SAMs that contain monodispersed nanometer- to micron-scale defects that are regularly spaced and sufficiently far apart that their diffusion layers do not overlap. In this case it is sometimes possible to determine detailed structural information about defects such as their number density and size; however, this situation is never realized experimentally. Interpretation is further complicated because the cyclic voltammetric response depends on the size, shape, and charge of the solution-phase probe molecule.[10] Thus, electrochemical methods are best used for *comparing* the average properties of SAMs or other thin films, rather than attempting to determine absolute defect configurations. In this section, we compare the cyclic voltammetric response of the three different-length SAMs prepared by both liquid- and vapor-phase deposition.

The cyclic voltammetric data shown in Figure 5 and Table IV were obtained for SAM-modified electrodes immersed in aqueous solutions consisting of 5 mM $Ru(NH_3)_6^{3+}$ and 1.0 M KCl. First, we compare the data for SAMs of the same thickness, but prepared from different ambients. Vapor-phase-deposited $Au/HS(CH_2)_5CH_3$ SAMs yield plateau-shaped cyclic voltammograms, which indicate the monolayer contains small defects that are sufficiently separated that their diffusion layers do not overlap. The same SAM prepared from the liquid phase yields a peak-shaped voltammogram, which indicates either many small, closely-spaced defect sites or a few much larger defects.[10] Qualitatively, we interpret the data to indicate that vapor-phase-deposited $Au/HS(CH_2)_5CH_3$ SAMs contain fewer and smaller defects than corresponding SAMs deposited from the liquid phase. This result is consistent with the STM data discussed previously.

The current densities measured for $Au/HS(CH_2)_{11}CH_3$ SAMs prepared from either liquid or vapor phases are approximately the same, whereas the STM results indicated that the vapor-phase deposited SAMs presented a better barrier to $CN^-$ penetration. We are confident that both data sets are correct, since we have repeated them several times and obtained the same results. To interpret the data it is necessary to remember that electron transfer between a solution-phase probe molecule and the substrate does not require intimate contact of the two, whereas direct contact between $CN^-$ and the substrate is required for Au dissolution. Considering this fact, we conclude that the $CN^-$-etching/STM method probes only a subset of the defects detected by the cyclic voltammetric experiment. Hence, the total number density of defects within the liquid- and vapor-phase-deposited

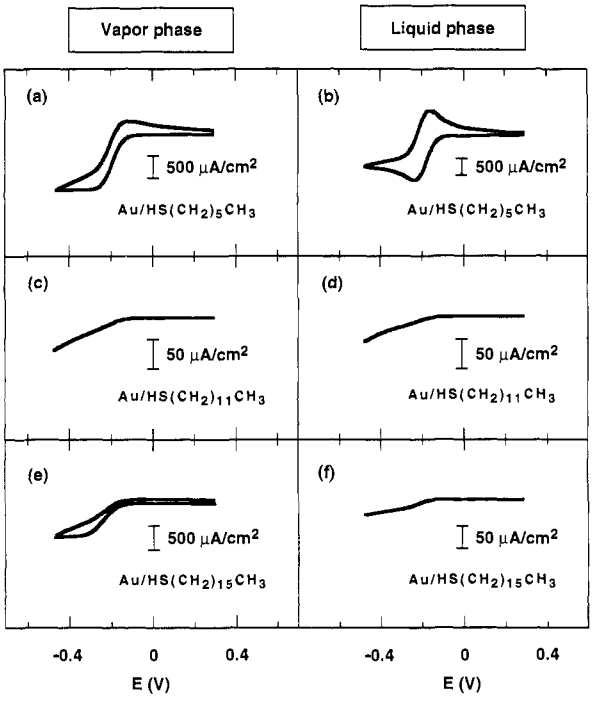


**Figure 5.** Cyclic voltammetric data obtained for 5.0 mM $Ru(NH_3)_6^{3+}$/1.0 M KCl electrolyte solutions at SAM-coated Au(111) electrodes: (a) vapor-phase-deposited $Au/HS(CH_2)_5CH_3$ SAM, electrode area ($A$) = $4.5 \times 10^{-4}$ cm²; (b) liquid-phase-deposited $Au/HS(CH_2)_5CH_3$ SAM, $A = 8.6 \times 10^{-4}$ cm²; (c) vapor-phase-deposited $Au/HS(CH_2)_{11}CH_3$ SAM, $A = 6.1 \times 10^{-4}$ cm²; (d) liquid-phase-deposited $Au/HS(CH_2)_{11}CH_3$ SAM, $A = 6.1 \times 10^{-4}$ cm²; (e) vapor-phase-deposited $Au/HS(CH_2)_{15}CH_3$ SAM, $A = 4.9 \times 10^{-4}$ cm²; (f) liquid-phase-deposited $Au/HS(CH_2)_{15}CH_3$ SAM, $A = 4.6 \times 10^{-4}$ cm². Scan rate: 0.1 V/s.

**Table IV.** Current Density as a Function of SAM Thickness and Deposition Medium

| SAM | current density ($\mu A/cm^2$)[a] | |
|---|---|---|
| | vapor phase | liquid phase |
| $Au/HS(CH_2)_5CH_3$ | 329 ± 16 (5) | 1130 ± 67 (7) |
| $Au/HS(CH_2)_{11}CH_3$ | 6 ± 1 (6) | 7 ± 4 (5) |
| $Au/HS(CH_2)_{15}CH_3$ | 155 ± 48 (6) | 4 ± 1 (6) |

[a] Data correspond to cyclic voltammograms like those shown in Figure 5. Current densities measured at –0.2 V for 5.0 mM $Ru(NH_3)_6^{3+}$/1.0 M KCl electrolyte solutions. Electrode areas were determined by analyzing optical micrographs. The error limits correspond to 1 $\sigma$ values calculated using the number of independent experiments shown in parentheses.

$Au/HS(CH_2)_{11}CH_3$ SAMs is approximately the same, but the vapor-phase-deposited SAMs contain less defects that penetrate completely through the SAM to the underlying Au surface.

The electrochemical data indicate that $Au/HS(CH_2)_{15}CH_3$ SAMs prepared from the vapor phase contain far more defects than the corresponding SAMs prepared from the liquid phase (Figure 5, parts e and f, respectively). This result is also in semiquantitative agreement with the STM results, which indicated that $Au/HS(CH_2)_{15}CH_3$ SAMs prepared from the vapor phase contained about 20 times more defects than the corresponding SAMs prepared from the liquid. We emphasize that these electrochemical experiments are fully reproducible: between 5 and 7 completely independent electrochemical experiments yielded essentially the same result for the liquid- and vapor-phase-deposited $Au/HS(CH_2)_{11}CH_3$ and $Au/HS(CH_2)_{15}CH_3$ SAMs.

The electrochemical behavior of the three different SAMs is quantitatively summarized in Table IV. Here, we compare the average current densities, which we measured at –0.2 V, that result from reduction of $Ru(NH_3)_6^{3+}$ at SAM-coated electrodes. Higher current densities reflect poorer SAM barrier behavior. The important result is that liquid-phase deposited SAMs contain less electroactive defects as the SAM thickness increases. In contrast, the short-chain, vapor-phase-deposited SAM is a better barrier than the corresponding liquid-phase-deposited SAM, but this trend reverses as the SAM thickness increases. These experimental results serve to reinforce the model we proposed based on the STM data.

## Conclusion

In this paper we have shown that when SAMs deposited from the liquid and vapor phases are probed using analytical methods having millimeter-scale lateral resolution, their structures are found to be identical. For example, FTIR-ERS and ellipsometry indicate that the thickness, structure, and packing densities of SAMs deposited from the two ambients are indistinguishable. These results are consistent with our previous nanogravimetric surface acoustic wave experiments, which indicated that precisely monolayer coverages of a range of organomercaptans irreversibly bind to Au surfaces from vapor-phase ambients.[1]

In contrast to these results, higher resolution STM and cyclic voltammetric data reveal some interesting differences between SAMs deposited from liquid and vapor phases. For example, we find that liquid-phase-deposited SAMs are better mass-transfer barriers than vapor-phase-deposited SAMs when the *n*-alkanethiols are relatively long, but that this behavior reverses for the shorter SAMs. We also find that thiol-induced changes in Au substrate morphology are different depending on the contacting ambient phase. Although speculation at the present time is premature, these observations may provide some insight into the mechanism of self-assembly, which is at present not understood. For example, data regarding structure and formation kinetics of SAMs in both media might lead to a microscopic understanding of how solvent intercalation, head- and tail-group solvation, and competition for adsorption sites by solvent affect the barrier and wetting properties of SAMs.

The data presented here also reveal some insight into the origin of the small cylindrical pits observed in SAMs by STM.[11,20,35] By combining the molecular specificity of electrochemistry with the high spatial resolution of STM we have been able to eliminate two possible pit-formation mechanisms that previously appeared quite reasonable: these cylindrical features do not arise from missing *n*-alkanethiol molecules, nor do they result from thiol-stimulated Au dissolution. Rather, we believe that SAMs alter the top-most layers of Au, probably through an energetically favorable surface restructuring and an enhanced Au surface diffusion rate. Other ions that strongly adsorb to Au are also known to have this effect, which is a consequence of an increased coordination number for Au when it is in the presence of strongly adsorbing ions.[26]

Our central conclusion that the macroscopic-scale differences between liquid- and vapor-phase-deposited SAMs are minimal should help to stimulate technological applications of SAMs and lead to a more detailed understanding of the self-assembly process.

**Acknowledgment.** This work is supported by the National Science Foundation (CHE-90146566) and the Office of Naval Research. We thank Professor Mark Bryant for helpful discussions.